Dosimetric double network hydrogel based on Poly(vinyl-alcohol)/Phenylalanine-derivatives with enhanced mechanical properties

Silvia Locarno[1,2], Salvatore Gallo[1,2,], Paolo Arosio[1,2], Chantal Biordi[1], David Dallasega[3], Marco Gargano[1], Nicola Ludwig[1], Francesco Orsini[1,2], Emanuele Pignoli[4], Ivan Veronese[1,2], Cristina Lenardi[1,2]*

[1] Dipartimento di Fisica "Aldo Pontremoli", Università degli Studi di Milano, Via Giovanni Celoria 16, 20133 Milano, Italy

[2] Istituto Nazionale di Fisica Nucleare (INFN) - Sezione di Milano, Milano, Italy

[3] Dipartimento di Energia, Politecnico di Milano, via Ponzio 34/3, 20133 Milano, Italy

[4] Fondazione IRCCS "Istituto Nazionale dei Tumori", via Venezian 1, 20133 Milano, Italy

Corresponding author: *Salvatore Gallo, Ph.D. e-mail: salvatore.gallo@unimi.it*
Dipartimento di Fisica, Università degli Studi di Milano, Via G. Celoria 16, 20133 Milano, Italy

Abstract

An innovative double network hydrogel based on Poly(vinyl-alcohol) (PVA) cross-linked with Glutaraldehyde (GTA) was obtained by the addition of self-assembling phenylalanine (Phe) derivatives with the aim to achieve improved mechanical-elastic properties exploitable to produce 3D dosimeters. The self-assembling ability in fibrous structures of Phe derivatives (FmocPhe-OH, A; FmocPhe-Phe-OMe, P) even within the PVA gel was proved by AFM and SEM imaging. The proposed matrices containing A and P were completely characterized from the physical-chemical point of view in order to deeply understand how the two molecules influenced the hydrogel properties. In particular, mechanical tests proved that the addition of the Phe derivatives produce higher stiffness, toughness and stretchability of the hydrogels. In particular, these properties appear in the peptide P matrix and could be appropriately tailored by regulating the concentration of the added molecule. Preliminary dosimetric studies were also performed by infusing the studied hydrogels with Fricke solution. P type has demonstrated to be suitable for dosimetric applications avoiding any effect on dose response of the hydrogel. This work presents an unconventional material able to provide clinicians and medical physicists with effective and reliable 3D dosimetric measurements for the development of anthropomorphic phantoms that mimic mechanical properties and radiological-response of human-tissues.

1. Introduction

Radiotherapy (RT) is one of the main treatment modalities for neoplastic lesions. The goal of RT is to deliver a prescribed radiation dose (which is the energy deposited in matter by ionizing radiation per unit mass) to a tumor site meanwhile minimizing the damage to healthy tissue[1]. The validation and radiation process control depends on the measurement of the absorbed dose, usually obtained with the use of dosimetric systems. The major limitation of this control, however, is the inability to perform in-depth investigation on the 3-dimensional (3D) spatial distribution of the radiation dose, which includes doses released in the healthy tissues.

Gel dosimetry, as Fricke gel (FG) dosimetry, has been widely studied for radiotherapy/radiosurgery applications because of their radiological tissue equivalence, ease of molding into any desired shape and size and therefore useful for evaluating the 3D relative dose distributions[2-4].

FG dosimeter is based on hydrogel matrices loaded with iron ions. The interaction of ionizing radiation produces the oxidation of ferrous ions (Fe^{2+}) into ferric ions (Fe^{3+}) with a yield proportional to the dose.

A 3D spatial dose-information is achievable within the gel volume, and it can be captured and retrieved by Magnetic Resonance Imaging (MRI)[5,6], since the two iron ions influence differently the nuclear relaxation times of the protons in the molecules surrounding them. Moreover, the addition of the metallic-ion indicator like as Xylenol Orange (XO)[7,8] to the Fricke gel dosimeters makes these materials suitable for being analyzed by 3D-optical CT scanners[9,10].

Besides the great advantages, some limits, such as the spatial and temporal instability of the dosimetric information, make this kind of dosimeter still inadequate for routine applications in the clinical environment. Various FG dosimeters are discussed in the literature based on different polymeric matrices and readout approaches in order to overcome these limits[2-4]. However, all the proposed hydrogel matrices still show lacks mechanical flexibility, in terms of ability of bending, folding and stretching together with high cracking and rupture resistance[11,12]. All these properties are of primary importance considering the necessity to prepare anthropomorphic phantoms with an elasticity comparable to various soft tissues of the human body, allowing, among others, the dosimetric application in sophisticated radiotherapy treatments for organs subjected to natural movement (*i.e.* breathing)[13-16].

In this work, a different strategy based on the formation of the double network structure consisting of two types of polymer obtained through the addition of self-assembling molecules, has been studied for improving mechanical-elastic properties of the hydrogel based on Poly(vinyl-alcohol) (PVA) chemically cross-linked by Glutaraldehyde (GTA). This matrix, in fact, has had a considerable increase in the use over the past 5 years for dosimetric pre-clinical applications[17-22]. In particular, two derivatives of the versatile amino acid phenylalanine (Phe), the amino acid Fmoc-Phe-COOH (A) and the peptide Fmoc-PhePhe-OMe (P), have been studied for the optimization of FG dosimeters. In fact, it is well known in the literature that Phe derivatives form a tubular structure with a length of 100 μm and longer through the formation of hydrogen bonding as well as *Van der Waals* interactions, electrostatic and π–π stacking of aromatic residues, depending on the chemical nature of the molecule[23-25]. These tubular structures could be exploited to form a secondary network in the PVA-GTA matrix since they are able to be easily deformed by mechanical stress or temperature

variation, interesting properties that could be exploited to mold the matrix to any desired shape[26]. Several examples of double network hydrogels with improved mechanical properties are reported in the literature[27–29]. Here, the self-assembly ability of Phe derivatives inside the gel has been evaluated and a complete characterization of the matrices has been provided in terms of their physical-chemical and morphological properties as well as of the mechanical behavior. Data have shown that even if both A and P type are able to self-assemble into the hydrogel matrix, the morphology of the two molecular architectures is completely different and only P type is able to modulate the mechanical properties as a function of its concentration. Encourage to this result, preliminary dosimetric analysis has been performed and the data confirmed that the inclusion of peptide P in a PVA based FG dosimeter do not affected its dosimetric features (in terms of dose-sensitivity), suggesting that peptide P is a promising candidate for improving the mechanical properties of the dosimetric hydrogels.

2. Materials and Methods

2.1 Materials

Fmoc-L-Phe-OH (**A**), 1-Ethyl-3-(3-dimethylaminopropyl)carbodiimide (EDC) and L-Phe-OMe were purchased from Iris Biotech. Hydroxybenzotriazole (HOBt), N,N-Diisopropylethylamine (DIPEA), PVA Mowiol®18-88 (molecular weight 130000 Da; degree of hydrolysis 86.7-88.7%, PVA), glutaraldehyde (GTA solution 25% v/v in water) were purchased from Sigma-Aldrich. Sulfuric acid (SA) was purchased by VWR. Ferrous ammonium sulfate hexahydrate (FAS) was purchased from Carlo Erba, while Xylenol Orange tetra-sodium sodium salt (XO) from Riedel-de Haën. All solvents were of ACS grade or higher and were obtained from Sigma-Aldrich. All batches of hydrogels were prepared using ultrapure water (resistivity 18.2 MΩ·cm) obtained by a water purification system (Milli-Q® Direct, EMD Millipore, Germany).

2.2 Synthesis of Fmoc-Phe-Phe-OMe (P)

Fmoc-L-Phe-OH (A, 0.5 g, 1.30 mmol) was dissolved in dichloromethane (DCM, 10 ml/mmol) at 0°C before adding EDC (1.1 eq, 1.42 mmol) and HOBt (1.1 eq, 1.42 mmol) and was stirred for 1 hour. Then, L-Phe-OMe (1.1 eq, 1.42 mmol) and DIPEA were added until pH=7-8. The mixture was allowed to react overnight at room temperature. The solvent was removed under reduced pressure. The residue was dissolved in DCM and the organic phase was washed with 5% w/v aqueous citric acid, saturated aqueous NaHCO$_3$ and brine. The organic layer was dried over Na$_2$SO$_4$, filtered and concentrated under reduced pressure. The crude product was crystallized from DCM/ethyl ether to afford the pure product. ^{1}H NMR spectra were recorded on Varian Gemini 300 using deuterated chloroform (CDCl$_3$) as solvent.
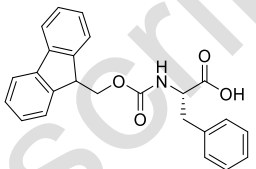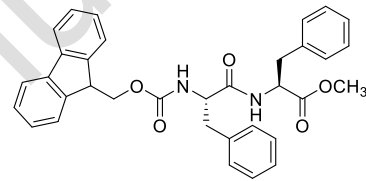
(0.65 g, 91%). White solid. νmax/cm-1 3330 (NH), 1693 (CO). 1H NMR (300 MHz, CDCl3) δ 2.96-3.11 (4H, m, CH2), 3.67 (3H, s, CH3), 4.16-4.21 (1H, m, CH), 4.27-4.45 (3H, m, CH, CH2), 4.74-4.81 (1H, m, CH), 6.17 (1H, br s, NH), 8.37 (1H, br s, NH), 6.94-6.97 (2H, m, ArylH), 7.18-7.38 (10H, m, ArylH), 7.38-7.43 (2H, m, ArylH), 7.51-7.55 (2H, m, ArylH), 7.77 (2H, d, J = 7.5 Hz, ArylH).

3

2.3 Hydrogels preparation

PVA stock solution was prepared by dissolving 10.6 g of PVA in 75 ml of ultrapure water, at 70 °C under moderate stirring (~150 rpm) for 40 minutes. The final concentration of PVA stock solution was 12.4% w/w. After the complete dissolution, the PVA solution was left to cool down at room temperature.

PVA hydrogels were obtained by adding 93.0 µL of SA to 54.8 g of PVA solution. Then, a different amount of water, dimethyl sulfoxide (DMSO) or DMSO solution of A (100 mg/ml) or P (100 mg/ml) was added. Details of the various sets of PVA hydrogels prepared were summarized in Table 1. Afterwards, the final concentration of PVA was adjusted at 9.1% w/w by adding an appropriate volume of ultrapure water, considering the different density of each component. Finally, GTA (660 µL) was added under magnetic stirring. The final concentrations of SA and GTA in the gel were 25.0 mM and 25.6 mM respectively. Figure SI0 shows a synthetic scheme of the sample preparation steps. After one minute of stirring to achieve homogeneity, the final solution was poured into UV-Vis standard cuvettes Poly(methyl-methacrylate) (10 mm optical path length) or into NMR-tubes (10 mm of inner diameter) and closed with stoppers and sealed with Parafilm™. After the complete gelation, all hydrogels were maintained in a refrigerator at the temperature of 6 °C.

Table 1. Details of the additive concentrations in the hydrogel samples.

Sample	Additive	[DMSO] (% w/w)	[A] or [P] (% w/w)
PVA-GTA	--	--	--
D1		2.0	--
D2	DMSO	4.0	--
D3		6.0	--
A1		2.0	0.20
A2		4.0	0.40
A3	FmocPhe-OH (A) 100 mg/ml in DMSO	6.0	0.60
P1		2.0	0.20
P2		4.0	0.40
P3	FmocPhe-Phe-OMe (P) 100 mg/ml in DMSO	6.0	0.60

2.4 Morphological assessments: AFM and SEM

In order to gain visual insight into the morphology of the hydrogels, scanning electron microscopy (SEM) and atomic force microscopy (AFM) were utilized.

SEM surface images were acquired with FE-SEM Zeiss Supra 40 equipped with the GEMINI column, operating at an accelerating voltage of 5 kV, in order to minimize charging effect of the polymeric samples. The samples have been air-dried and the surface has not been prepared or covered with any conductive film

(carbon or gold) that could hide the presence of the fibers. In addition, a high resolution *in lens* detector has been used to detect the fibers inside the hydrogel matrix.

AFM imaging was performed in air using a Nanoscope Multimode IIId system (Bruker, Santa Barbara, CA, USA) operating in tapping-mode. For this measurement, the samples were in the form of the wet hydrogels AFM images were collected using the RMS amplitude of the cantilever as the feedback signal for the vertical sample position. The RMS free amplitude of the cantilever was approximately 15 nm and the relative set-point above 95% of the free amplitude. Rectangular silicon probes with nominal spring constant around 2.5 N/m (NT-MDT, Russia), typical tip curvature radius of 10 nm and cantilever length of 120 μm were used. The cantilever resonance frequency was about 130 kHz. Images were recorded at ~1 Hz line rate and a resolution of 512x512 pixels per image was chosen. AFM images were subjected to a line-by-line subtraction of linear background to eliminate sample tilt from the images and corrected for stepwise changes between individual scan lines. The r.m.s. surface roughness was evaluated from several AFM topography images collected in different areas on the PVA gel surface.

2.5 Vibrational IR spectroscopy

FT-IR spectra were recorded with FT-IR FAME Analyzer, composed of a Frontier™ ATR FT-IR spectrometer, on samples in xerogel form, operating in free air conditions and at room temperature (20 ± 2°C). Spectra were acquired from 4000 to 650 cm^{-1} at a resolution of 4 cm^{-1} with 120 scans per sample.

2.6 Contact angle/wettability and evaporative rate

Contact angle experiments were carried out by syringing 2 mg of ultrapure water droplet using a micropipette set up at 2 microliters on the hydrogel surface and observing the droplet with a portable microscope (Dino-Lite AM4013MZ, 5 MP variable magnification ratio up to 220x, polarized light), using the 35x magnification ratio. The images were acquired on fresh gels and on gels maintained in isolated and controlled environment, in order to minimize water losses, within 48 hours after their preparation. The measurements of the contact angle were assessed using *ImageJ software* equipped with the contact angle plugin in the manual mode. The obtained data were averaged over 4 repetitions. As far as the evaporation flux concerned, the weight of the gels was measured by a 10^{-4} *g* precision balance (Mettler-Toledo).

2.7 ^{1}H-NMR relaxometry measurements

^{1}H NMR relaxometric characterization was carried out using a Stelar Spinmaster Fourier transform NMR spectrometer. The ^{1}H-NMR relaxometry broadband measurements were performed at room temperature (23.0 ± 1.0 °C) on gel samples directly formed inside the sample holder by measuring the longitudinal and the transverse nuclear relaxation times T_1 and T_2. NMR data were collected at a magnetic field (frequency) of 1.0 T (42.58 MHz) using Saturation Recovery (SR) and Carr Purcell-Meiboom Gill pulse sequences for longitudinal relaxation time T_1 and transverse relaxation time T_2 measurements, respectively. Instead, as recommended in the literature[30], for what concerns the dosimetric aspect the attention was paid to the T_1 values.

5

2.8 Gel fraction determination

Each piece sample was placed in an oven (Thermo Scientific oven Heraeus Function Line Series) at 37 °C until constant weight was reached before the gel fraction (GF%) measurements. Then, each sample was immersed into ultrapure water at room temperature for 4 days to rinse away un-reacted species. Subsequently, the immersed sample was removed from distilled water and dried at 37 °C until constant weight was reached. Therefore, the gel fraction could be calculated as follows:

$$GF\% = \frac{W_f}{W_i} \cdot 100 \qquad (1)$$

where W_i and W_f are the weights of the xerogels before and after the immersion, respectively.

2.9 Gel swelling degree measurements

Swelling determinations were carried out in ultrapure water at 25 °C. All samples were dried before immersion at 37 °C for 48 h. The equilibrium swelling degree (M%) was determined as follows:

$$M\% = \frac{M_f - M_i}{M_i} \cdot 100 \qquad (2)$$

where M_i is the weight of the samples before immersion and M_f is the weight of the sample at equilibrium water content.

2.10 Gel water loss measurements

To perform water loss (WL%) measurements, each piece of sample was placed at room temperature and weighted at set times. The water loss was determined as follows:

$$WL\% = \frac{W_t}{W_i} \cdot 100 \qquad (3)$$

where W_t and W_i are the weights of the samples at the setting and initial time, respectively.

2.11 Mechanical characterization

Stress and strain tests were performed at room temperature and a crosshead speed of 30 mm/min. (100 cycles for each sample), using a digital Sauter dynamometer FH 50 with integrated measuring cell and RS-232 data interface. The wet hydrogels were cut with a rectangular shape (20×0.3×50 mm) and clamped to the machine. The Young's modulus (E), the stress-at break (σ_{max}) and maximum elongation-at-break (ε) were recorded.

2.12 Fricke hydrogel-dosimeters preparation

The PVA-GTA FG dosimeters with and without DMSO or solution of A or of P in DMSO were prepared using 0.50 mM of FAS; 0.165 mM of XO, 25.6 mM of GTA and 25 mM of SA. Figure SI0 shows a pattern of the Fricke hydrogel-dosimeters preparation steps. Details on the final concentrations are shown in Table SI1 (*see* Supporting Information).

2.13 Dose response measurements

UV-Vis cuvettes and NMR-tubes with FG dosimeters were uniformly irradiated by means of an Irradiator for Biological Materials IBL-437C at the *"Fondazione IRCCS Istituto Nazionale dei Tumori"* of Milano (Italy) at room temperature. Considering the source activity and the irradiation geometry, the dose rate at the sample positions was evaluated equal to 11 Gy/s, as also attested by inter-comparison measurements with calibrated medical linear accelerators available in the same institute using various types of dosimeters, including Fricke gel dosimeters. For all sets of dosimeters, the investigated dose interval was 0.0-20.0 Gy, *i.e.* the range of interest in typical radiotherapy applications. For each dose value, at least triplicates of samples were irradiated. The Optical Absorbance (O.A.) spectra of the samples were acquired in the wavelength range 360-720 nm with the step of 1 nm and using ultrapure water as blank. Optical absorbance spectra were acquired using an UV-Vis spectrophotometer (Cary 100 UV-Vis, Agilent Technologies, Santa Clara, CA, USA). The spectra were the average of 20 samples from the same set.

According to the indications in the literature [31], the UV-Vis measurements were performed at least one hour after the irradiation. For quantitative analysis, the integral of O.A. variation Σ(O.A.), *i.e.* sum of ΔO.A. between 480 and 620 nm was chosen as a dosimetric parameter. Furthermore, the values of ΔO.A. at 555 nm were used for reconstructing the dose-response curve [32]. The dose response ^{1}H-NMR measurements were performed as explained in 2.8 for non-irradiated samples.

3. Results and Discussion

3.1 Self-assembly study in the hydrogel network

The PVA-GTA matrix with the addition of Fmoc-L-Phe-OH (A) or Fmoc-Phe-Phe-OMe (P) was prepared according to the protocol described in the Materials and Methods, section 2.3. The water-insoluble self-assembling molecules were dissolved in dimethyl sulfoxide (DMSO) at a concentration of 100 mg/ml. Then, their stock solutions were diluted in acidic PVA and water solution until reaching the final desired concentration shown in Table 1. The concentration of SA in the final solution was 25.0 mM (corresponding to a pH value about 1.5). The mixture was stirred until a homogeneous solution was obtained and finally was cross-linked by GTA.

3.1.1 Morphological analysis by AFM and SEM

The surface morphology of PVA-GTA hydrogels was investigated by Tapping Mode Atomic Force Microscopy (TM-AFM). Figure 1 shows the AFM topography images of PVA gels with amino acid A and with peptide P, while the reference images of PVA-GTA and D3 samples are reported in Figure SI1. Fiber-like structures were visualized on the surface of A samples where both the number and the length of single fibers increased with the amino acid concentration (the vertical scale in Figure 1a is the same for all the AFM images in order to facilitate their comparison).

Fiber-like structures appeared to be homogeneously distributed on the whole gel surface without a well-defined orientation and with a mean diameter in the order of tens of nanometers. Moreover, some fibers showed 90 degree bending in their conformation as well visible in AFM images. On the other hand, the fiber-like structures of PVA gels with the addition of peptide P were not so well-defined as in A samples, thus suggesting their presence mainly in deeper layers of the PVA hydrogels. Fibers appeared to be, however, arranged in a more ordered pattern with a defined orientation, indicating a different supramolecular organization/arrangement.

On the contrary, AFM images of PVA-GTA and D3 (the sample having the highest DMSO concentration) did not reveal any identifiable morphological structure (Figure SI1), confirming that even within the gel, the two molecules maintained the self-assembly ability in fibrous structure, allowing the formation of a double network hydrogel[23,24].
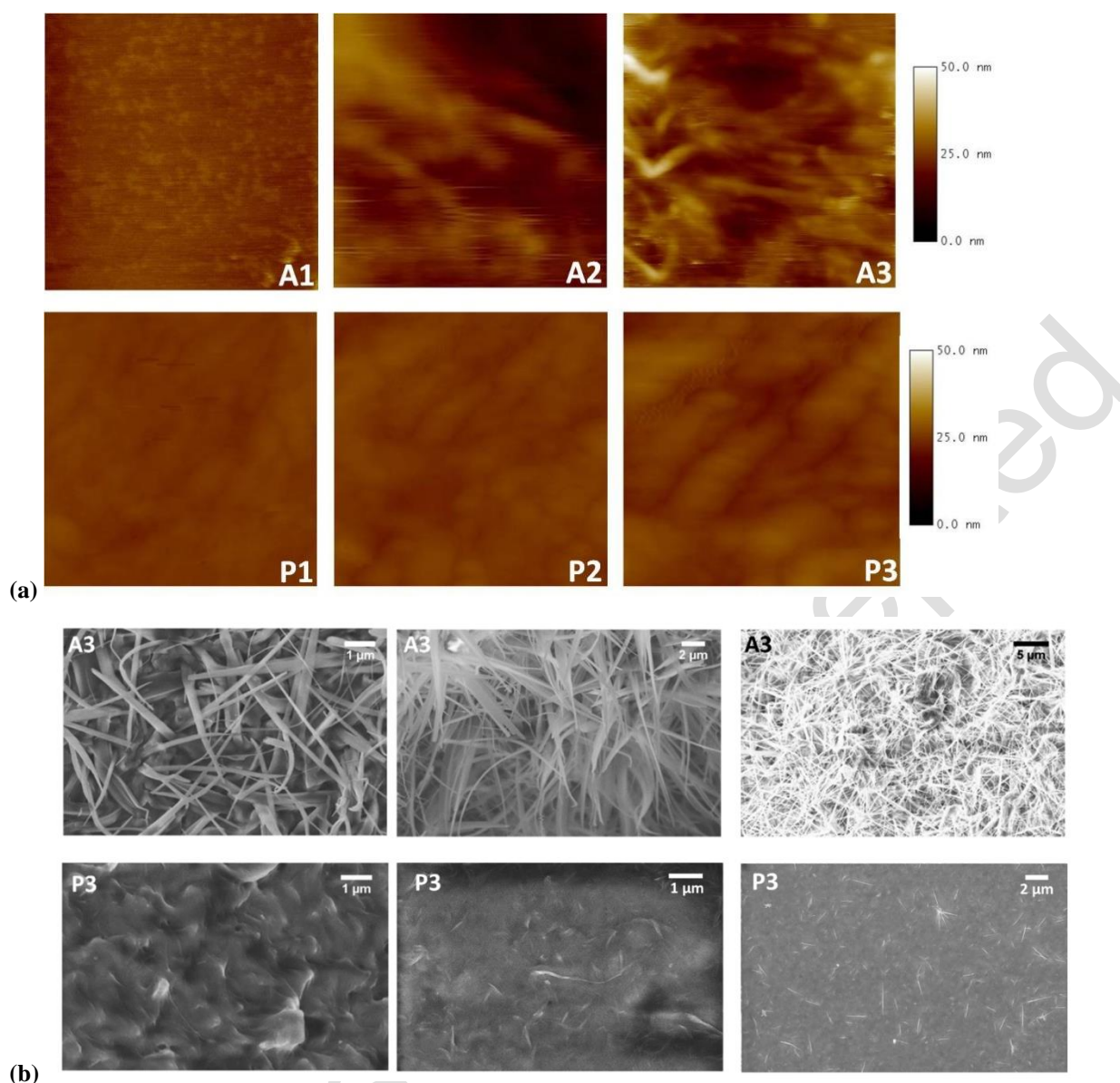
8

Figure 1. (a) AFM topography images of hydrogel samples with the addition of A (upper images; samples A1, A2, A3 from left to right) and P (lower images; samples P1, P2, P3 from left to right). Scan area 1x1 μm²; and vertical (color) scale 50 nm for all the images. **(b)** SEM micrographs of the surfaces-hydrogel-samples with different magnifications. Top row: A3 sample, bottom row: P3 sample.

AFM analysis also allowed us to quantitatively evaluate the hydrogel r.m.s. surface roughness, as reported in Table SI2. PVA-GTA and D3 samples, as expected, exhibited the lowest values of r.m.s. roughness, whereas A and P samples showed higher values with a comparable growth trend as a function of the concentration. The presence of many fiber-like structures on the surface of the studied samples has to be considered in the evaluation of the r.m.s. surface roughness values reported in Table SI2. In fact, as expected, the higher r.m.s surface roughness matches the samples prepared with increased amino acid and peptide concentration (A2, A3 and P2, P3), for which the number, the length and the height of the fiber-like structures increased as observed in Figure 1a.

9

The different morphology of the PVA hydrogels appeared even more evident with the SEM imaging. SEM micrographs were acquired on the xerogels with the highest additives concentration (Figure 1b for A3 and P3 and Figure SI2 for PVA-GTA and D3). The images confirmed that A formed a superficial layer of fibers with an average diameter of around 100 nm several microns long protruding out of the sample surface, responsible for the opacity of the hydrogel. Conversely, P formed thinner fibers that appeared to be embedded into the gel and promoted the formation of an anisotropic matrix.

It is worth noticing that similar fiber-like structures covering the surface of the studied samples were observed with two different techniques: AFM imaging showed fiber-like structures at nanometer level, densely distributed on the whole surface often overlapped each other and bended as well as, at micrometer scale, similar structures were observed in SEM micrographs as shown in Figure 1a and Figure 1b for samples A3 and P3.

3.1.2 Chemical Bonding Analysis

In order to better understand the chemical nature and conformation of A and P type structures included in PVA based hydrogel, vibrational infrared spectra were acquired in solid state and compared with the spectra of PVA-GTA hydrogel and of the molecules reference powder (Figure 2). The specific features of the additive molecules clearly arise in the samples including A (Figure 2a) and P (Figure 2b), indicating that the two molecules, even dispersed in the matrix, maintained the same chemical identity and configuration of the powder.

For both additives, distinguishing peaks appeared in the wavenumber region among 1800-1600 cm⁻¹, which corresponds to the C=O stretching vibrations of the amide, urethane and ester groups. In the case of amino acid A (Figure 2a), in addition to the C=O stretching band peaked at 1693 cm⁻¹, another stretching band at 1729 cm⁻¹ was found, that corresponds to non-hydrogen bonded carbonyl carbamate of Fmoc group [24].

Moreover, in A powder, the two C=O vibrations presented similar intensity while in the gel, regardless of amino acid concentration, the non-hydrogen bonded stretching strongly lost relative intensity while the band at 1693 cm⁻¹ was slightly downshifted (-4 cm⁻¹). This suggested considerable hydrogen bonding of carbonyl carbamate to PVA neighboring molecules, which are rich in OH groups. On the other hand, no variations were observed at the level of the N–H-stretching whose band was found at 3330 cm⁻¹. Concerning the foot-printing region below 1500 cm⁻¹, the phenyl bending vibrations were more defined when the molecule was inside the gel, probably because π-π stacking between the aromatic rings of the amino acid facilitated the formation of well-ordered structures.

The IR spectra of peptide P (Figure 2b) showed the tendency of the molecule to self-assemble into β-sheets as confirmed by the sharp peaks at 1699 and 1646 cm⁻¹ which were related to the presence of β-sheet structures[25]. Their formation was promoted and stabilized by the hydrogen bonds, especially in the gel where numerous hydrogen bond acceptor groups (OH) were present. As a matter of fact, the non-hydrogen bonded C=O vibration at 1736 cm⁻¹ was less intense in the gel than in the power. The most informative region for P containing samples ranged among 3500-3200 cm⁻¹, which corresponds to N-H stretching vibrations of the amide and N-protecting urethane groups. Moreover, the amide group was also involved in the hydrogen

bonding network that stabilized the fiber structure of the peptide as evidenced by the N–H stretching band redshift (from 3330 to 3300 cm^{-1}). The presence of stronger hydrogen bonds in P type hydrogel than in A hydrogel might be a consequence of the fact that P fibers were located in the deep layer of the gel, as emerged from the morphological analysis. Thus, P molecules were closely in contact with PVA OH groups and the hydrogen bond formation was facilitated. In the foot printing region of peptide P, some differences in the band intensities were observed between the spectra of the powder and of the gels, as the out-of-plane bending of aromatic moieties at 950 cm^{-1} attributed to the molecular reorientation into the gel network. Finally, the gel spectra with peptide showed two peaks at 2900 and at 2800 cm^{-1} due to the presence of DMSO solvent [33]. DMSO bands were not found, instead, in the gel spectra with amino acid A, suggesting that gel containing P retained a greater amount of solvent molecules than those containing A.
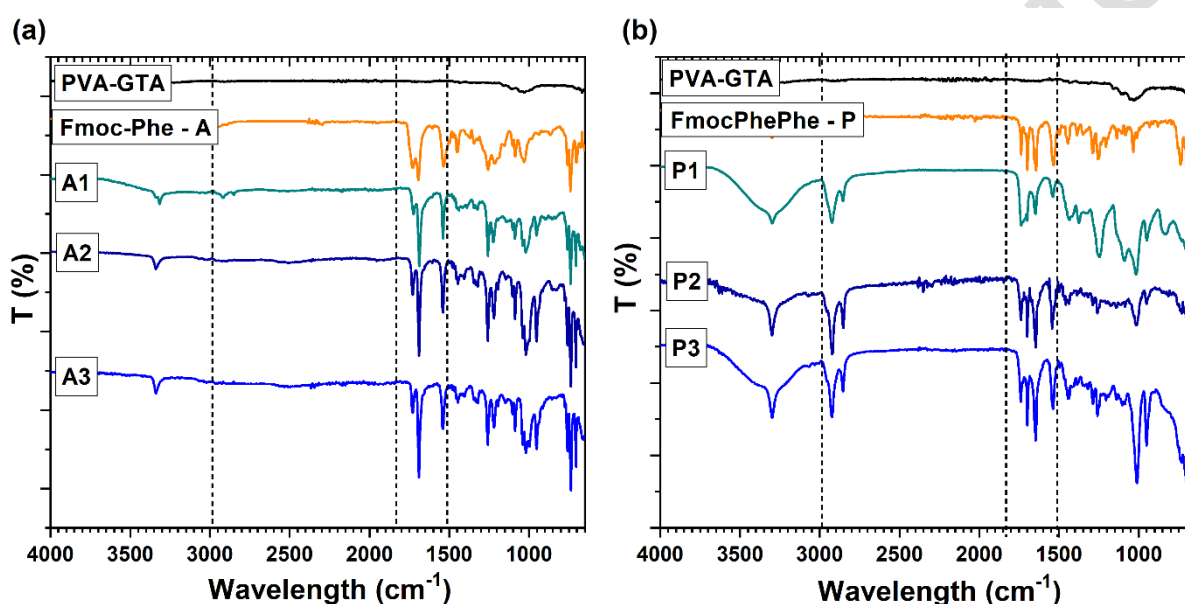

Figure 2. IR spectra of xerogel samples containing (a) amino acid A and (b) peptide P. The spectra of PVA-GTA sample and of A or P powder were used as reference.

3.2 Physical-chemical characterization of the double network hydrogels

3.2.1 Gel fraction and Wettability

The crosslink efficiency of the hydrogel network was evaluated by gel fraction (GF%) experiments. The GF% of PVA-GTA reached 95% (Table 4), indicating that almost all the polymeric subunits became connected. When DMSO was added, the GF% decreased by increasing the DMSO concentration (D series in Table 2). This demonstrated that DMSO molecules do not participate in the gel network and they were free to spread out. The high boiling point of DMSO (189 °C), in fact, did not allow the evaporation of DMSO molecules during the gel drying process at 37 °C. As a consequence, when the xerogel was swollen in water, the free DMSO molecules, started to spread out of the matrix driven by the concentration gradient. The degree of the GF% decrease reflected the amount of DMSO added to the PVA gels that has been lost during the swelling in water. On the other hand, with the addition of amino acid A and peptide P, the GF% was lower respect to

PVA-GTA, because of the presence of DMSO, but it was greater with respect to samples loaded only with DMSO, confirming that the Phe derivatives formed the secondary gel network through fiber structures.

Table 2. GF%, contact angle and instantaneous surface evaporation rate of hydrogel samples. The last two analyses were conducted on fresh gel and repeated after 48 hours on the same samples.

Sample	GF%	Inner contact angle (deg)		Instantaneous Evaporation rate (mg/min)	
		Fresh gel	After 48 h	Fresh gel	After 48 h
PVA-GTA	94.9 ± 1.4	78.09 ± 3.22	77.26 ± 1.70	2.25 ± 0.18	2.48 ± 0.24
D1	78.4 ± 0.7	--	--	--	--
D2	70.2 ± 1.0	--	--	--	--
D3	70.1 ± 1.4	74.05 ± 3.14	86.97 ± 3.89	1.75 ± 0.12	2.40 ± 0.12
A1	84.0 ± 2.9	80.36 ± 0.96	81.95 ± 0.85	--	--
A2	79.5 ± 4.0	86.79 ± 0.62	83.66 ± 1.51	--	--
A3	78.3 ± 3.6	86.12 ± 0.53	79.65 ± 0.77	1.05 ± 0.04	0.76 ± 0.04
P1	81.8 ± 2.0	80.70 ± 1.72	77.46 ± 0.12	--	--
P2	77.9 ± 3.9	86.56 ± 0.32	71.15 ± 0.81	--	--
P3	74.1 ± 0.8	84.28 ± 0.74	71.80 ± 0.62	1.07 ± 0.02	0.78 ± 0.02

Another important property of the hydrogel is the wettability that is the results of the complex effects of different features such as roughness, chemical composition and how the range of the intermolecular forces causes an equilibrium condition where the surface may or may not be wetted by the liquid. Wettability can be investigated through the measure of the contact angle (*see* Table 2), which is the angle formed between a liquid drop (*e.g.* purified water) and a solid surface (*e.g.* hydrogel surface) when they come in contact together. This angle is determined by the liquid-solid interface interaction. For PVA-GTA the contact angle did not change in a period of 48 hours, whereas the sample containing only DMSO (D3) exhibited an increase in the angle of about 13 deg after 48 hours, indicating a tendency to decrease the surface wettability over time.

The fresh samples with amino acid (A series) showed a slightly lower wettability with respect to reference sample PVA-GTA and the measured contact angle was preserved also after 48 hours.

Also the fresh peptide-based gels (P series) showed similar values to those of A samples, whereas after 48 hours exhibited a decrease of the contact angle, reaching a value of about 16 deg less for the sample P3, so attesting an appreciable increment of the wettability.

Evaporation rate was also evaluated in order to have critical information on gel decay. Evaporation rate is the amount of vapor leaving the sample surface during a certain time. In solid porous materials it depends on the porous network inside the material (size and connection) and on how the water can reach the surface moving inside it by capillary or by diffusion. Evaporation rates were evaluated only for the PVA-GTA hydrogel and for the samples containing the larger amount of additives (D3, A3 and P3, *see* Table 2). A3 and P3 samples showed the tendency to reduce their own rate after 48 hours, with respect to formulations containing only PVA-GTA and DMSO (D3), indicating and confirming the formation of a more interconnected network with

respect to the hydrogel without self-assembling molecules. The increase of the evaporation rate after 48 hours in PVA-GTA and D3 samples could be attributed either to the change in hydrogel structure due to sample dryness and to the formation of micro-fractures on the surface, since both effects could lead to the augmentation of the evaporating rate through the extension of the open pores surface. This result suggested that self-assembling molecules (A3 and P3) imparted a less fragility to the hydrogel.

3.2.2 Local spin dynamics analysis

The local spin dynamics of the system was deeply investigated by ^{1}H-NMR relaxometry experiments. In particular, the NMR nuclear relaxation times, T_1 and T_2, are two important parameters related to the relaxation process of the hydrogen nuclear magnetization and depend on the interaction between the hydrogen nuclei and the surrounding environment (*i.e.* other magnetic moments and all the other factors able to interact with the spins of the hydrogen nuclei, like chemical functional groups, electron density and so on). In the analyzed samples most hydrogen nuclei were water protons, therefore the obtained ^{1}H-NMR signal reflected the information coming from the interaction of different water molecules inside the gels with the other components of the sample. Bearing this in mind, the effect of the gelling process was investigated by analyzing the relaxation curves of the transverse nuclear magnetization obtained at ν=42.58 MHz (*i.e.* a magnetic field of $\mu_0H = 1T$). Figure 3a shows the transverse decays of the samples D2, A2 and P2. Trend similar to the A2 curve was observed for the samples A1 and A3 and to the P2 curve for the samples P1 and P3. The plot of the exponential decays in a semi-log scale clearly exhibited the non-linearity of the curves, see the inset where the first 400 ms of decays were plotted.

Therefore, the curves indicated the presence of more than one component that constitute the T_2 exponential decays and could be roughly ascribed to the different environments that influence the nuclear relaxation of the spins of hydrogen nuclei (*i.e.* short T_2 components are related to best efficient interactions between hydrogen nuclei and the surrounding environment, vice versa for long T_2 components). In this sense the ^{1}H NMR relaxometry also detected the contributions caused by the different confinement of the water molecules inside the samples and confirmed the progressive organization of them starting from D2, passing to P2 and A2 [34,35]. Indeed, the decay curves clearly show the fastening of the nuclear relaxation for P2 and A2 with respect to D2 due to enhanced interactions with the *"surrounding world"*.
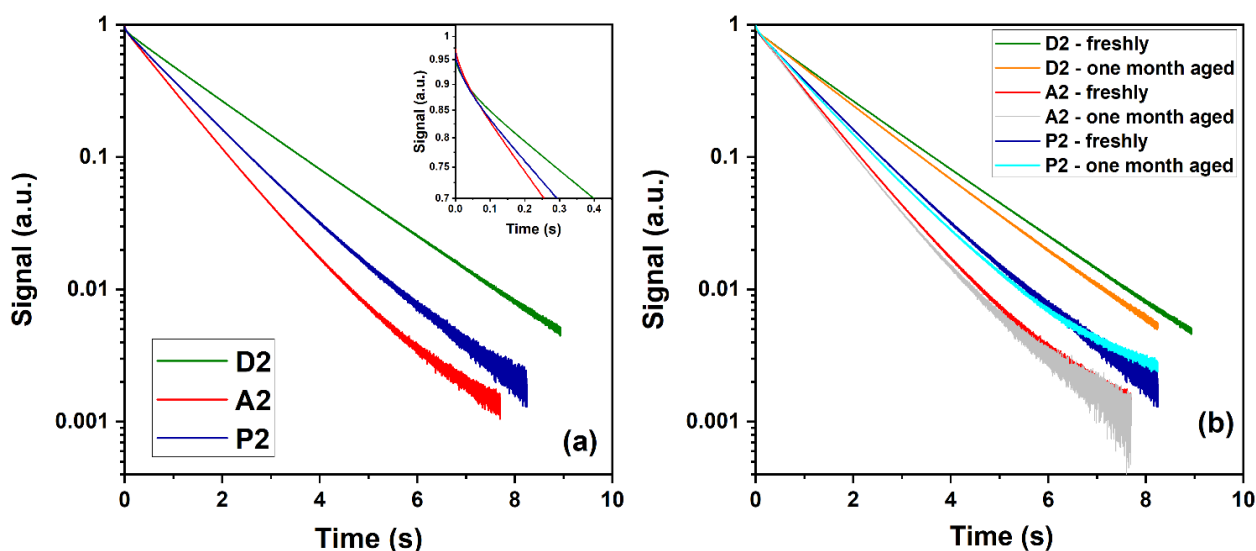
13

Figure 3. (a) Nuclear transverse relaxation curves for D2(green), A2 (red), P2 (dark blue). In the inset the first 400 ms of the same curves. (b) Nuclear transverse relaxation curves for hydrogel samples as prepared (D3, green; A2, red; P2, blue) and one month later (D2, orange; A2, light-grey; P2, cyan).

Another intriguing result obtained by ¹H-NMR relaxometry regarded the aging study of the proposed gel formulations. As it could be evidenced by the transverse decays shown in Figure 3b, the measurements performed one month later exhibit that the aging process had a moderate effect on the relaxometric properties of P2 and A2 samples. On the contrary, the decay curve of D2 shows a more pronounced effect. This last result was particularly interesting for proposed hydrogels shelf-life in view of practical application. During these steps, the samples were stored at 6 °C and sealed to prevent the water loss.

3.2.3 Hydrogel interactions with the surrounding environment

One of the main characteristics of hydrogels is their ability to swell in water without dissolving. When the hydrogel is in contact with the solvent molecules, the meshes of the hydrogel start expanding allowing the solvent molecules to penetrate within the polymeric network. The swelling process is driven by the favorable osmotic force and the opposite elasticity force, which balances the stretching of the network and prevents its deformation[36]. Table 3 shows the swelling degree results in ultrapure water. A slight trend could be observed as a function of the DMSO amount, probably because the DMSO concentration gradient promoted the penetration of the water molecules inside the gel. Whereas no significant variations within the experimental error range were observed between the different samples containing the same concentration of DMSO, suggesting that the Phe derivatives did not impact meaningfully the water absorption capacity of the PVA-GTA hydrogel.

Table 3. Swelling degree values of hydrogel samples.

Sample	Swelling degree (%)
PVA-GTA	198.2 ± 8.4
D1	175.1 ± 6.9
D2	196.3 ± 9.2
D3	224.0 ± 4.2
A1	180.6 ± 5.5
A2	193.5 ± 6.7
A3	212.9 ± 7.2
P1	171.8 ± 7.4
P2	193.9 ± 7.4
P3	212.7 ± 7.1

The difficulty in storing PVA-GTA hydrogel in air at ambient temperature (~25 °C) and humidity was probably caused by the high percentage of water that the gel loses in a short period of time (a few hours). In fact, as shown in Figure 4 already after 2 hours, the gel lost 13.0% of water and after 4 hours the 25.0% (black). Same values were found for the samples containing DMSO (Figure SI3). In Figure 4 the water loss of only D3 (green) is reported to make the graph easier to read. The behavior of these samples indicated that DMSO molecules did not influence the hydrogel capacity to lose/hold water. With the addition of the amino acid A (samples A, red) the gel ability to retain water was slightly increased but no significant increment was observed (water loss around 12.0% after 2 hours and around 23.0% after 4 hours). On the other hand, with the addition of peptide P (group samples P, blue) a more marked water retention of the gel was observed. In fact, after 2 hours the hydrogel lost only around 8.0% of water, while 15.0% after 4 hours, with a small variation between the samples with different concentrations of P, confirming a better stability of these hydrogels at room temperature.

After 2 days, all the hydrogel samples were completely dry and all the water evaporated. The PVA-GTA and D3 samples reached the same final weight (around 11.0% respect the initial one), while A and P samples kept a higher weight (around 20.0% respect the initial one). These results suggested and confirmed that DMSO was not part of the gel network while A and P types collaborated to the hydrogel matrix formation.
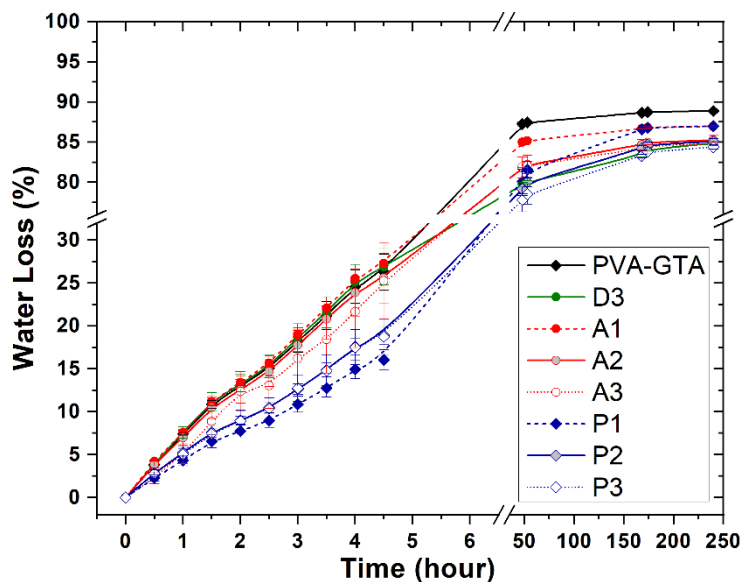
Figure 4. Water loss (%) as a function of time for hydrogel samples (PVA-GTA, black; D3, green; A series, red; P series, blue).

3.3 Mechanical characterization of the hydrogels

In order to evaluate the effect of the self-assembling molecules on the hardness of the gel, a systematic study of the mechanical properties of the prepared wet hydrogels was performed.

First of all, the deformation recoverability was evaluated by cyclic tests. All the samples were subjected to 100 stretching cycles and the acquired data indicated that all of them had an elastic behavior. In fact, the last value of stress did not change with the increase of loading cycles and the gels returned to their initial shape and size when the force was removed (*see* Figure SI4). Only the first cycle had an observable hysteresis loop, especially for samples loaded with A, and it became negligible for the following cycles, where constant resilience was observed. Furthermore, in Figure 5 the stress - strain curves under cyclic loading show that the hysteresis, related to the energy dissipation, is almost negligible for gel matrix containing only DMSO or A, whereas is slightly more evident in the case of P. This behavior, although it does not appear to be a clear discriminating factor, can be considered as evidence of different types, strengths and orientations of the material bonds. However, the most evident ameliorations induced by the addition of the amino-acid and peptide were the material hardening and that the failure point taked place at significantly higher stress/strain values with respect to pure and DMSO-containing matrix. This is particularly relevant for the sample P3 (see Figure 5) which appears to resemble the behavior of nanotubes embedded in polymers and attributed to the inclusion/distribution of fibers inside the matrix[37], as in the present case.

The tensile stress-strain curves of the samples D, A and P with different amounts of additives, all compared with PVA-GTA hydrogel, are shown in Figure 5 (panel a, b and c). For these samples, straight lines were fitted to the experimental data (stress *vs* strain) with the aim to evaluate the Young's modulus (E, Table 4) as linear coefficient of linear regression.

16

The addition of DMSO alone (D series, Figure 5a) did not influence the mechanical properties of the PVA-GTA hydrogel, in fact, E values slightly increased with an increase of DMSO amounts, remaining however below 30 kPa. This suggested that the samples loaded with DMSO alone have comparable toughness, within the experimental errors, with PVA-GTA hydrogel. On the other hand, the addition of self-assembling amino acid A (A series, Figure 5b) increased considerably the E value of the hydrogel, reaching more than 60 kPa, which was the highest value obtained compared with all other tested samples. Thus, A imparted the highest toughness but, however, it was not directly proportional to its concentration, therefore, it could not be easily modulated.

However, very interesting and promising results were obtained with the addition of peptide P (P series, Figure 5c). In particular, increasing P concentration led to a systematic higher stiffness and toughness of the double network hydrogel, suggesting that the mechanical properties could be fine tailored by adjusting the peptide amount, within the investigated concentration range.
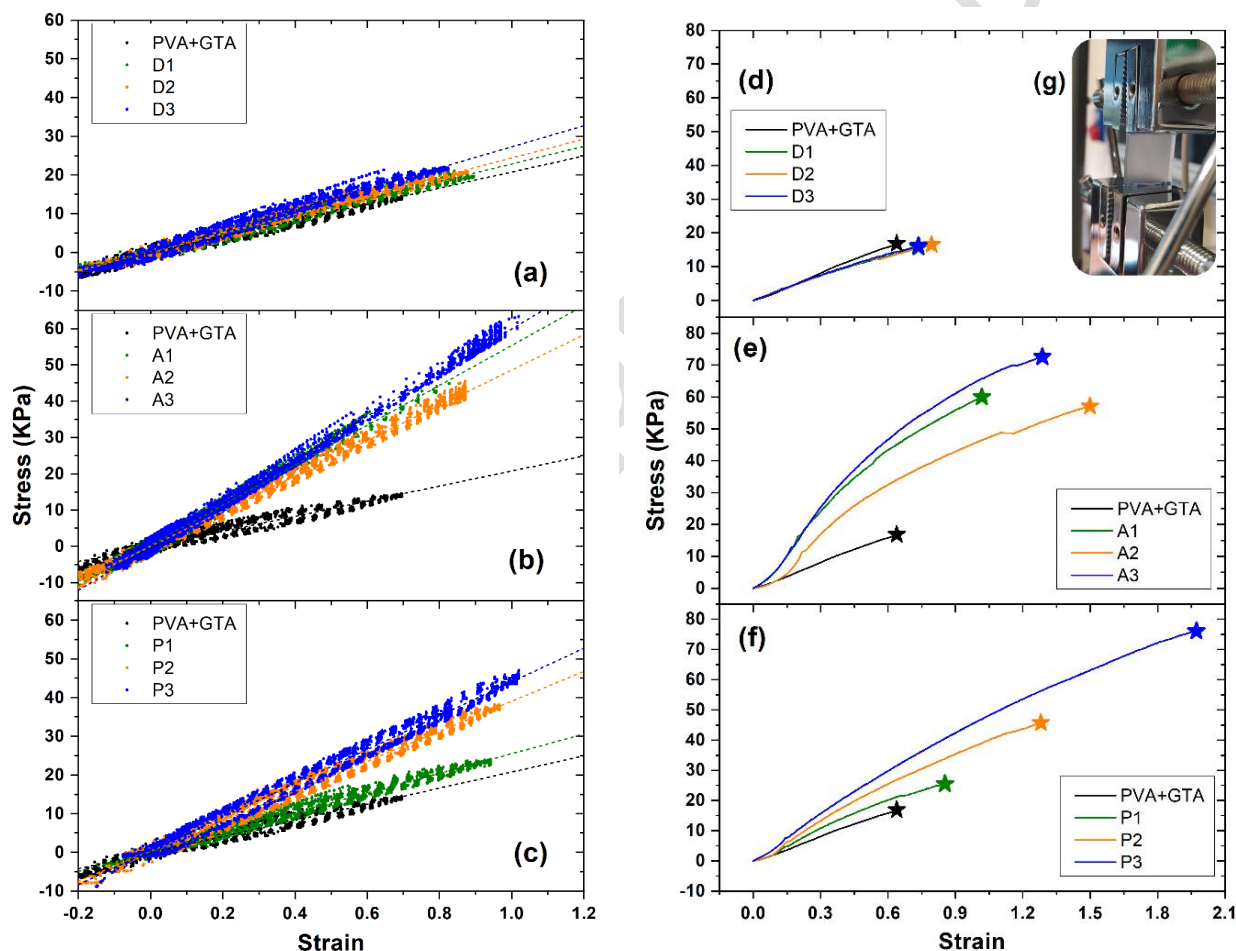

Figure 5. Tensile stress-strain curves of the samples D (a), A (b) and P (c), compared with PVA-GTA hydrogel. The dashed lines represent the fit curves extended across the graph as a guide for the eye. Stress-strain curves refer to breaking strength tests of samples D (d), samples A (e) and samples P (f) compared with PVA-GTA hydrogel. (g) Image of P2 sample subjected to tensile stress-strain experiment.

17

Table 4. Mechanical properties of tested hydrogels. The Young's modulus (E) values were calculated by fitting the linear region of the stress-strain curves in Figure 5.

Sample	E (KPa)	Breaking load (N)	Limit elongation (mm)
PVA-GTA	21.8 ± 4.1	1.0 ± 0.2	8.9 ± 1.7
D1	22.4 ± 1.8	0.8 ± 0.1	10.3 ± 0.8
D2	22.0 ± 2.3	0.8 ± 0.1	11.1 ± 1.2
D3	23.1 ± 3.2	0.8 ± 0.1	10.3 ± 1.4
A1	66.3 ± 5.4	3.1 ± 0.2	14.2 ± 1.2
A2	44.6 ± 3.8	2.9 ± 0.2	20.9 ± 1.8
A3	66.0 ± 5.1	3.7 ± 0.3	18.0 ± 1.4
P1	32.5 ± 0.7	1.3 ± 0.1	11.9 ± 0.6
P2	38.8 ± 3.7	2.3 ± 0.2	17.9 ± 1.7
P3	45.7 ± 4.5	3.9 ± 0.4	27.6 ± 2.7

The breaking strength test was also performed on all hydrogel samples in order to evaluate the tensile load required to fracture them. Each sample was subjected to 10 stretching cycles in order to remove the hysteresis loop and then, the tensile load was increased until breaking. Each experiment was repeated at least 3 times. The stress-strain curves obtained are shown in Figure 5 and the mechanical properties are summarized in Table 4. Figure 5 (panel d, e and f) showed the typical nonlinear stress-strain curve of an elastomer (polymer with viscoelasticity and with weak intermolecular forces), which generally possessed low E value and high failure strain compared with other materials.

Additionally, the obtained data confirmed that mechanical properties were not influenced by the presence of DMSO, in fact, also the stress-at-break and the maximum elongation-at-break of samples D were comparable, within the experimental errors, with those of PVA-GTA hydrogel. As far as samples A concerned, the greatest toughness was reached independently from the A concentration and this result was compliant with the behavior observed for the E values measurements. Figure 5f, instead, confirmed that the addition of peptide P increased the strength of the PVA gel as a function of the P concentration and sample P3 reached the highest limit elongation, enduring the greatest stress load.

3.4 Preliminary dosimetric characterization

3.4.1 Optical dose-response

In order to test the possible dosimetric applications of the implemented composite hydrogels, FAS and XO were added to these novel hydrogel matrices. These two reagents, in fact, in an acidic environment and within a tissue-equivalent hydrogel matrix, are able to create Fricke gel (FG) dosimeters.

After verifying that the addition of FAS and XO did not influence either the double network of resultant hydrogels or their mechanical features, the hydrogel matrices loaded with a Fricke solution were studied by optical absorption spectroscopy in order to evaluate the effects of various additives on their dosimetric properties. First of all, a systematic study on the DMSO concentration (from 0.0 to 10.0% w/w) was carried

18

out for evaluating the solvent effect on dosimetric response. As far as the samples with A and P, only 0.4% w/w concentration was chosen (A2 and P2), since the higher concentration (0.6% w/w) made the hydrogel too opaque to be analyzed by optical techniques (%T lower than 1%).

Unexpectedly, sample A2 completely oxidized in a few minutes and, consequently, the violet XO-Fe^{3+} complex appeared even without the irradiation. This intensive oxidation of Fe^{2+} was attributed to the presence of the free carboxylic group of A, which could interfere with the ferric ions oxidation and chelation [38,39]. As proof of this hypothesis, the esterification of the carboxylic group of A was carried out (*see* SI for reaction details). The esterification product (Fmoc-Phe-OEt) showed to be able to prevent the pre-irradiation Fe^{2+} oxidation even at higher concentration (0.6% w/w). However, the addition of Fmoc-Phe-OEt to the PVA-GTA hydrogel at any concentrations made the sample too opaque for the optical analysis. As a consequence, only additive P at the concentration of 0.4% w/w (FG-P) was considered suitable for optical dosimetry, since the ester group at the C-terminus inhibited the Fe^{2+} auto-oxidation and the hydrogel appeared transparent enough. The optical absorbance spectra after irradiation of the selected samples are shown in Figure SI5.
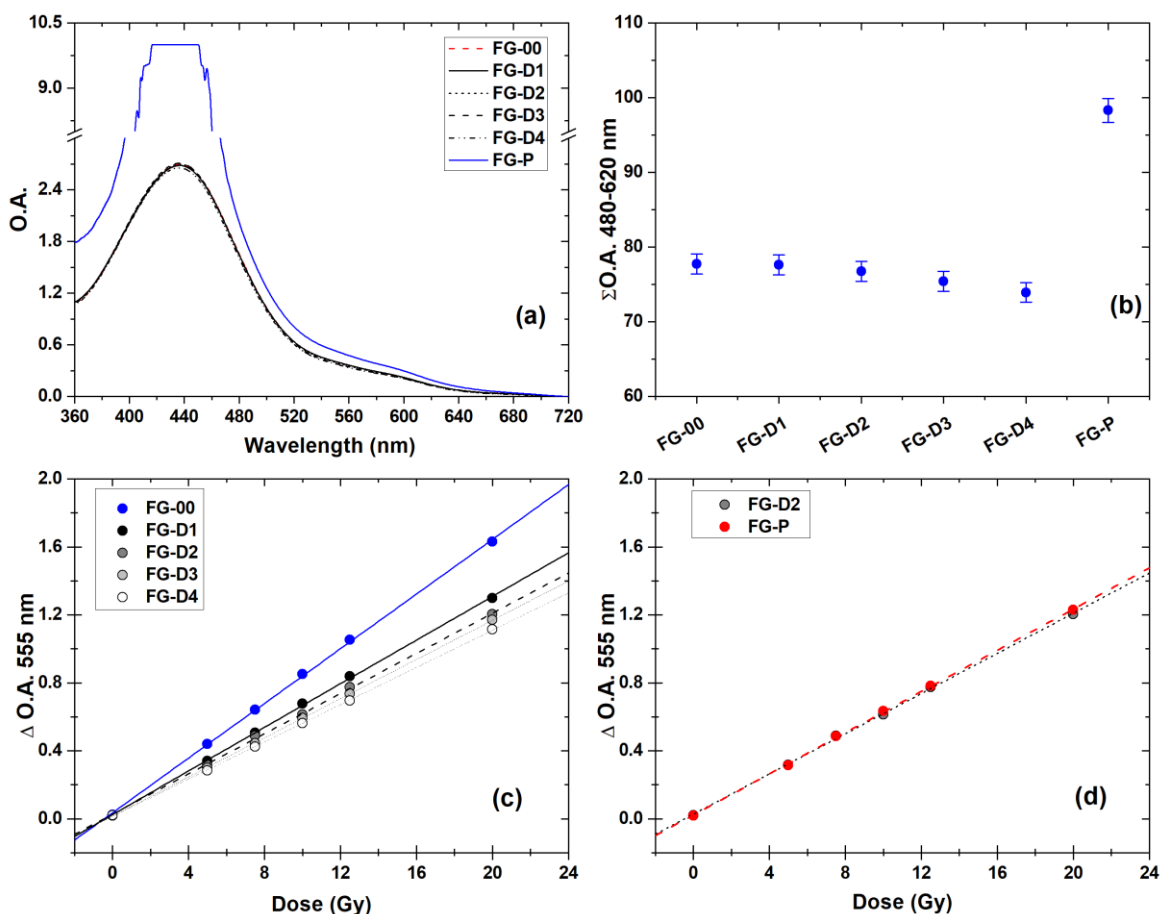

Figure 6. (a) O.A. spectra between 360-720 nm of the various types of un-irradiated Fricke gel. (b) Cumulative OA between 480-620 nm of FG in panel (a). Error bars correspond to one standard deviation. (c) O.A. variation at 555 nm of the various types of Fricke gel in cuvettes irradiated at increasing doses in the 0.0-20.0 Gy interval with different DMSO amounts. (d) Comparison between O.A. variation at 555 nm of FG-D2 and FG-P *vs* dose. The error bars are smaller than the size of the circles. The lines are the linear fits to the experimental data.

Figure 6a shows the optical absorbance spectrum between 360 nm and 720 nm for un-irradiates PVA-GTA-FG samples with and without additives. The OA spectra of all the samples, except for FG-P appeared overlapped (Figure 10a). All samples had an optical absorbance peak around 430 nm attributable to the free XO [21,40]. Samples enriched with P had an absorption band around 430 nm which cannot be quantified due to instrumental saturation. This aspect should be highlighted, but it is not significant for dosimetric evaluations. Conventionally in gel dosimetry, the spectral region of interest is yellow-green (500-600 nm).

Figure 6b shows the cumulative optical absorbance between 480 and 620 nm relating to panel (a). These values were comparable within experimental errors for all samples with and without DMSO. This allowed us to assert that DMSO did not influence the initial optical absorbance of the samples in the spectral region of dosimetric interest. Contrariwise, P type increased the initial O.A throughout the spectral region considered, and the experimental data were not comparable within the experimental errors, due to the opacity of the sample induced by the fiber structures of P samples.

Figure SI5 shows the O.A. variation (ΔO.A.) of spectra, due to irradiation, of all the studied dosimeters. These spectra were characterized by a broad absorption peak in the wavelength region between 500 nm and 600 nm. The shapes of spectra showed a main absorption around 585 nm, with a shoulder extending in the lower wavelength region (500-560 nm). As known from the literature, this broad band was due to the convolution of two peaks (520 and 585 nm) due to the different complexation of the XO with the ferric ions [21,40].

For a fixed dose value, the relative intensity of the absorption band with respect to the side shoulder changed with the gel composition. Indeed, the optical absorbance between 500 nm and 600 nm proved to decrease with increasing the DMSO concentration in the gel matrix.

As expected, the ΔO.A. of FG dosimeters without DMSO increased with increasing the radiation dose in the wavelength region between 480 nm and 660 nm. Similarly, a decrease of the ΔO.A. around 430 nm with increasing the radiation dose occurred. Such features could be observed also for the FG dosimeters containing DMSO, suggesting that the solvent did not impair the operating principle of the dosimeters and their optical analyses. Similar considerations could be made for the FG-P sample. The FG-P sample, in fact, showed the wide absorption band for wavelengths above 500 nm. This band grew as the dose given increased. No behavior could be found for wavelengths below 450 nm where the samples showed an instrumental saturation.

The plot of ΔO.A. at 555nm (average value ± one standard deviation calculated over three samples) versus dose, together with the straight lines fitted to the experimental data are shown in Figures 6c and 6d for FG dosimeters with different amount of DMSO and with and without P, respectively. The corresponding fit parameters are reported in Table SI3 (*see* Supporting Information).

The fitted straight lines in Figure 6c provided a good description of the experimental data over the entire considered dose interval. The sensitivities values (*i.e.* slopes of the fitted straight lines of Figure 6c) relate to different DMSO concentrations were not comparable within the experimental errors. The increase in the concentration of DMSO in the matrix caused a significant decrease in the optical dosimetric sensitivity of the FG dosimeters. For example, the use of DMSO at 2.0% w/w caused a reduction of about 20% which exceeded

32% for the concentration of DMSO 10.0% w/w. However, the decrease was not proportional to the concentration of DMSO used.

The influence of DMSO on the dose response was consistent with its free radical scavenger nature[41]. In fact, after irradiation, water decomposition occurs inside the hydrogel, according to the radiolysis process. As a consequence, hydroperoxy radicals are formed and Fe^{2+} ions are oxidized into Fe^{3+} ions. Therefore, free radicals play an important role in the oxidation of Fe^{2+} ions. Consequently, it is understandable that the sensitivity of FG hydrogels with the free radical scavenger DMSO was lower than the samples where free radical scavengers were not added[42], in fact, DMSO could capture free radicals (Figure 6). These results are in agreement with those obtained for standard XO-PVA-FG (irradiated at doses below 3 Gy)[43].

Additionally, it must be noted that the addition of P did not affect the optical dosimetric sensitivity. The FG-D2 sample had a comparable sensitivity within experimental errors with that of the FG-P sample. The two sets differed only in the presence of P, while they have the same amount of DMSO. Using the unpaired *t*-test, confidence levels of 22% could be estimated considering the data pairs FG-D2 and FG-P.

3.4.2 NMR dose-response

After the irradiation, the amount of Fe^{2+} ions converted to Fe^{3+} ions in the FG could be evaluated by means of MRI [5]. Indeed, the oxidation process caused a shortening of the longitudinal nuclear magnetic relaxation time (T_1) and a consequent increase of spin–lattice relaxation rate ($R_1=1/T_1$). For this reason, a T_1-weighted MRI could clearly distinguish between regions that received a different absorbed dose and could be used to deduce the dosimetric distribution. Similarly, to R_1, the spin–spin relaxation rate ($R_2=1/T_2$) of the FG dosimeter changed with variations in the absorbed dose [5,30].

Within this framework, T_1 of FG-00, FG-D2, FG-P irradiated at doses of 0.0, 7.0 and 14.0 Gy were evaluated by NMR relaxometry and the difference in the longitudinal relaxation rate ΔR_1 between the irradiated samples ($R_{1,0}=1/T_{1,0}$) and the un-irradiated samples ($R_{1,I}=1/T_{1,I}$) was estimated. Considering the fact that the slope of the straight line passing through ΔR_1 vs dose represented the dosimetric sensitivity of the samples, linear regressions of the data was performed.

Sensitivity values of 0.026 ± 0.001, 0.013 ± 0.001 and 0.017 ± 0.001 ($s^{-1}Gy^{-1}$) were obtained for samples FG-00, FG-D2 and FG-P, respectively (*see* Table SI3 in Supporting Information). These results confirmed that the presence of DMSO reduced (more than 50%) the dosimetric sensitivity of the samples, as already obtained by optical measurements.

Furthermore, it was possible to assert that DMSO lowered the production yield of Fe^{3+} ions and not the formation yield of the XO-Fe^{3+} optical complex. The dosimetric sensitivity of the FG-P sample was approximately 20% higher than that of the FG-D2 sample. This variation could be ascribable to the different matrices and the different confinement of the water they contain.

These results showed that the addition of the P in the matrix by means of a DMSO solution did not significantly modify the dosimetric properties of the FG in terms of optical sensitivity and in terms of NMR sensitivity.

4. Conclusions

In this paper, an innovative double network hydrogel based on PVA chemically cross-linked with GTA was characterized and proposed for a new approach to dosimetric applications. The novelty of the system consists in adding self-assembling Phe derivatives to the hydrogel with the aim to create a secondary network and, consequently, to impart greater mechanical resistance to the gel matrix. This research was, in fact, triggered by the stringent need to improve the handability of hydrogel-based dosimeters, mainly in terms of elasticity and stretchability. The addition of self-assembling FmocPheOH (A) and FmocPhe-Phe-OMe (P) appeared to be a viable way to achieve this purpose, due to the molecules ability to form fibrous structures. Both molecules imparted mechanical properties to the material to make it sufficiently tough and extensible miming natural deformation occurring in organs and phantoms during radiation exposures. Differently only P conferred the ability to regulate mechanical properties as a function of its amount regardless of DMSO content. DMSO was in fact essential to convey A and P in the gel ensuring their solubility in water. However, the experimental results showed that this solvent was not part of the gel network and did not impact on gel properties. The different mechanical performances of A and P types were attributed to the different morphology and distribution of the fibrous structures, since, while A formed a superficial layer of fibers, P promoted the formation of an anisotropic matrix in deeper layers inside the gel. Moreover, the addition of P to the PVA based gel provided a greater stability at room temperature.

The achieved improvement of the mechanical-properties made PVA hydrogel more resistant, allowing better handling and making these materials very appealing for specific clinical applications.

In order to assess the dosimetric response of the hydrogel composite, preliminary dosimetric validation was performed by means of Optical Absorbance spectroscopy and NMR relaxometry techniques. The overall results indicated a slight loss of sensitivity due to the DMSO as free radical scavenger.

Additional investigations appear to be necessary to obtain deeper evaluation in the dosimetric response of the studied systems in terms of sensitivity and stability. Further tests in clinical settings are also required for determining their performance in 3D assessment of the dose.

Associated Content

*Supporting Information

The Supporting Information is available free of charge at https://pubs.acs.org/doi/zzzzzzxxxxx.

Additional experimental results, such as the SEM and AFM images of PVA-GTA sample, ^{1}H NMR of D samples, Synthesis of Fmoc-Phe-OEt, tables of data, a brief discussion about stress-strain curve and comparison tables.

Author Contributions

The manuscript was written through contributions of all authors. All authors have given approval to the final version of the manuscript.

References

(1)   Kron, T.; Fox, C.; Ebert, M. A.; Thwaites, D. Quality Management in Radiotherapy Treatment Delivery. *J. Med. Imaging Radiat. Oncol.* **2022**, *66* (2), 279–290. https://doi.org/10.1111/1754-9485.13348.

(2)   Marrale, M.; D'Errico, F. Hydrogels for Three-Dimensional Ionizing-Radiation Dosimetry. *Gels* **2021**, *7* (2), 74. https://doi.org/10.3390/gels7020074.

(3)   De Deene, Y. Radiation Dosimetry by Use of Radiosensitive Hydrogels and Polymers: Mechanisms, State-of-the-Art and Perspective from 3D to 4D. *Gels* **2022**, *8* (9), 599. https://doi.org/10.3390/gels8090599.

(4)   Macchione, M. A.; Lechón Páez, S.; Strumia, M. C.; Valente, M.; Mattea, F. Chemical Overview of Gel Dosimetry Systems: A Comprehensive Review. *Gels* **2022**, *8* (10), 663. https://doi.org/10.3390/gels8100663.

(5)   MacDougall, N. D.; Pitchford, W. G.; Smith, M. A. A Systematic Review of the Precision and Accuracy of Dose Measurements in Photon Radiotherapy Using Polymer and Fricke MRI Gel Dosimetry. *Phys. Med. Biol.* **2002**, *47* (20), R107–R121. https://doi.org/10.1088/0031-9155/47/20/201.

(6)   Gore, J. C.; Kang, Y. S. Measurement of Radiation Dose Distributions by Nuclear Magnetic Resonance (NMR) Imaging. *Phys. Med. Biol.* **1984**, *29* (10), 1189–1197. https://doi.org/10.1088/0031-9155/29/10/002.

(7)   Rae, W. I. D.; Willemse, C. A.; Lötter, M. G.; Engelbrecht, J. S.; Swarts, J. C. Chelator Effect on Ion Diffusion in Ferrous-Sulfate-Doped Gelatin Gel Dosimeters as Analyzed by MRI. *Med. Phys.* **1996**, *23* (1), 15–23. https://doi.org/10.1118/1.597787.

(8)   Gallo, S.; Cremonesi, L.; Gambarini, G.; Ianni, L.; Lenardi, C.; Argentiere, S.; Bettega, D.; Gargano, M.; Ludwig, N.; Veronese, I. Study of the Effect of Laponite on Fricke Xylenol Orange Gel Dosimeter by Optical Techniques. *Sensors Actuators, B Chem.* **2018**, *272*. https://doi.org/10.1016/j.snb.2018.05.153.

(9)   da Silveira, M. A.; Pavoni, J. F.; Bruno, A. C.; Arruda, G. V.; Baffa, O. Three-Dimensional Dosimetry by Optical-CT and Radiochromic Gel Dosimeter of a Multiple Isocenter Craniospinal Radiation Therapy Procedure. *Gels* **2022**, *8* (9), 582. https://doi.org/10.3390/gels8090582.

(10) Rousseau, A.; Stien, C.; Bordy, J.-M.; Blideanu, V. Fricke-Xylenol Orange-Gelatin Gel Characterization with Dual Wavelength Cone-Beam Optical CT Scanner for Applications in Stereotactic and Dynamic Radiotherapy. *Phys. Medica* **2022**, *97*, 1–12. https://doi.org/10.1016/j.ejmp.2022.03.008.

(11) Calvert, P. Hydrogels for Soft Machines. *Adv. Mater.* **2009**, *21* (7), 743–756. https://doi.org/10.1002/adma.200800534.

(12) Haque, M. A.; Kurokawa, T.; Gong, J. P. Super Tough Double Network Hydrogels and Their Application as Biomaterials. *Polymer (Guildf).* **2012**, *53* (9), 1805–1822.

https://doi.org/10.1016/j.polymer.2012.03.013.

(13) Yeo, U. J.; Taylor, M. L.; Dunn, L.; Kron, T.; Smith, R. L.; Franich, R. D. A Novel Methodology for 3D Deformable Dosimetry. *Med. Phys.* **2012**, *39* (4), 2203–2213. https://doi.org/10.1118/1.3694107.

(14) De Deene, Y.; Skyt, P. S.; Hil, R.; Booth, J. T. FlexyDos3D: A Deformable Anthropomorphic 3D Radiation Dosimeter: Radiation Properties. *Phys. Med. Biol.* **2015**, *60* (4), 1543–1563. https://doi.org/10.1088/0031-9155/60/4/1543.

(15) Du, Y.; Wang, R.; Yue, H.; Zhang, Y.; Wu, H.; Wang, W. Dose Response and Stability of Silicone-Based Deformable Radiochromic Dosimeters (FlexyDos3D) Using Spectrophotometer and Flatbed Scanner. *Radiat. Phys. Chem.* **2020**, *168*, 108574. https://doi.org/10.1016/j.radphyschem.2019.108574.

(16) Wheatley, M. J.; Balatinac, A. S.; Booth, J. T.; De Deene, Y. Physico-Chemical Properties and Optimization of the Deformable FlexyDos3D Radiation Dosimeter. *Phys. Med. Biol.* **2018**, *63* (21), 215028. https://doi.org/10.1088/1361-6560/aae7e7.

(17) d'Errico, F.; Lazzeri, L.; Dondi, D.; Mariani, M.; Marrale, M.; Souza, S. O.; Gambarini, G. Novel GTA-PVA Fricke Gels for Three-Dimensional Dose Mapping in Radiotherapy. *Radiat. Meas.* **2017**, *106*, 612–617. https://doi.org/10.1016/j.radmeas.2017.07.003.

(18) Lazzeri, L.; Marini, A.; Cascone, M. G.; D'Errico, F. Dosimetric and Chemical Characteristics of Fricke Gels Based on PVA Matrices Cross-Linked with Glutaraldehyde. *Phys. Med. Biol.* **2019**, *64* (8), 085015. https://doi.org/10.1088/1361-6560/ab135c.

(19) Gallo, S.; Gambarini, G.; Veronese, I.; Argentiere, S.; Gargano, M.; Ianni, L.; Lenardi, C.; Ludwig, N.; Pignoli, E.; d'Errico, F. Does the Gelation Temperature or the Sulfuric Acid Concentration Influence the Dosimetric Properties of Radiochromic PVA-GTA Xylenol Orange Fricke Gels? *Radiat. Phys. Chem.* **2019**, *160*. https://doi.org/10.1016/j.radphyschem.2019.03.014.

(20) Gallo, S.; Lizio, D.; Monti, A. F.; Veronese, I.; Brambilla, M. G.; Lenardi, C.; Torresin, A.; Gambarini, G. Temperature Behavior of Radiochromic Poly(Vinyl-Alcohol)-Glutaraldehyde Fricke Gel Dosimeters in Practice. *J. Phys. D. Appl. Phys.* **2020**, *53* (36). https://doi.org/10.1088/1361-6463/ab9265.

(21) Scotti, M.; Arosio, P.; Brambilla, E.; Gallo, S.; Lenardi, C.; Locarno, S.; Orsini, F.; Pignoli, E.; Pedicone, L.; Veronese, I. How Xylenol Orange and Ferrous Ammonium Sulphate Influence the Dosimetric Properties of PVA–GTA Fricke Gel Dosimeters: A Spectrophotometric Study. *Gels* **2022**, *8* (4), 204. https://doi.org/10.3390/gels8040204.

(22) Collura, G.; Gallo, S.; Tranchina, L.; Abbate, B. F.; Bartolotta, A.; D'Errico, F.; Marrale, M. Analysis of the Response of PVA-GTA Fricke-Gel Dosimeters with Clinical Magnetic Resonance Imaging. *Nucl. Instruments Methods Phys. Res. Sect. B Beam Interact. with Mater. Atoms* **2018**, *414*, 146–153. https://doi.org/10.1016/j.nimb.2017.06.012.

(23) Draper, E. R.; Morris, K. L.; Little, M. A.; Raeburn, J.; Colquhoun, C.; Cross, E. R.; McDonald, T. O.; Serpell, L. C.; Adams, D. J. Hydrogels Formed from Fmoc Amino Acids. *CrystEngComm* **2015**, *17* (42), 8047–8057. https://doi.org/10.1039/C5CE00801H.

(24) Singh, V.; Snigdha, K.; Singh, C.; Sinha, N.; Thakur, A. K. Understanding the Self-Assembly of Fmoc–Phenylalanine to Hydrogel Formation. *Soft Matter* **2015**, *11* (26), 5353–5364. https://doi.org/10.1039/C5SM00843C.

(25) Reches, M.; Gazit, E. Self-Assembly of Peptide Nanotubes and Amyloid-like Structures by Charged-Termini-Capped Diphenylalanine Peptide Analogues. *Isr. J. Chem.* **2005**, *45* (3), 363–371. https://doi.org/10.1560/5MC0-V3DX-KE0B-YF3J.

(26) Dudukovic, N. A.; Zukoski, C. F. Mechanical Properties of Self-Assembled Fmoc-Diphenylalanine Molecular Gels. *Langmuir* **2014**, *30* (15), 4493–4500. https://doi.org/10.1021/la500589f.

(27) Huang, X.; Li, J.; Luo, J.; Gao, Q.; Mao, A.; Li, J. Research Progress on Double-Network Hydrogels. *Mater. Today Commun.* **2021**, *29*, 102757. https://doi.org/10.1016/j.mtcomm.2021.102757.

(28) Sun, H.; Zhang, M.; Liu, M.; Yu, Y.; Xu, X.; Li, J. Fabrication of Double-Network Hydrogels with Universal Adhesion and Superior Extensibility and Cytocompatibility by One-Pot Method. *Biomacromolecules* **2020**, *21* (12), 4699–4708. https://doi.org/10.1021/acs.biomac.0c00822.

(29) Gong, J. P. Why Are Double Network Hydrogels so Tough? *Soft Matter* **2010**, *6* (12), 2583. https://doi.org/10.1039/b924290b.

(30) Marrale, M.; Brai, M.; Longo, A.; Gallo, S.; Tomarchio, E.; Tranchina, L.; Gagliardo, C.; D'Errico, F. NMR Relaxometry Measurements of Fricke Gel Dosimeters Exposed to Neutrons. *Radiat. Phys. Chem.* **2014**, *104*. https://doi.org/10.1016/j.radphyschem.2014.05.049.

(31) Marini, A.; Lazzeri, L.; Cascone, M. G.; Ciolini, R.; Tana, L.; d'Errico, F. Fricke Gel Dosimeters with Low-Diffusion and High-Sensitivity Based on a Chemically Cross-Linked PVA Matrix. *Radiat. Meas.* **2017**, *106*, 618–621. https://doi.org/10.1016/j.radmeas.2017.02.012.

(32) Gallo, S.; Artuso, E.; Brambilla, M. G.; Gambarini, G.; Lenardi, C.; Monti, A. F.; Torresin, A.; Pignoli, E.; Veronese, I. Characterization of Radiochromic Poly(Vinyl-Alcohol)-Glutaraldehyde Fricke Gels for Dosimetry in External x-Ray Radiation Therapy. *J. Phys. D. Appl. Phys.* **2019**, *52* (22). https://doi.org/10.1088/1361-6463/ab08d0.

(33) Wallace, V. M.; Dhumal, N. R.; Zehentbauer, F. M.; Kim, H. J.; Kiefer, J. Revisiting the Aqueous Solutions of Dimethyl Sulfoxide by Spectroscopy in the Mid- and Near-Infrared: Experiments and Car–Parrinello Simulations. *J. Phys. Chem. B* **2015**, *119* (46), 14780–14789. https://doi.org/10.1021/acs.jpcb.5b09196.

(34) Watson, A. T.; Chang, C. T. P. Characterizing Porous Media with NMR Methods. *Prog. Nucl. Magn. Reson. Spectrosc.* **1997**, *31* (4), 343–386. https://doi.org/10.1016/S0079-6565(97)00053-8.

(35) BROWN, RJS; FATT, I. MEASUREMENTS OF FRACTIONAL WETTABILITY OF OILFIELD ROCKS BY THE NUCLEAR MAGNETIC RELAXATION METHOD. *Trans. Am. Inst. Min. Metall. Eng.* **1956**, *207* (11), 262–264.

(36) Theoretical Description of Hydrogel Swelling: A Review. *Iran. Polym. J.* **2010**, *19* (5), 375–398.

(37) Esmaeili, A.; Sbarufatti, C.; Ma, D.; Manes, A.; Jiménez-Suárez, A.; Ureña, A.; Dellasega, D.; Hamouda, A. M. S. Strain and Crack Growth Sensing Capability of SWCNT Reinforced Epoxy in Tensile and Mode I Fracture Tests. *Compos. Sci. Technol.* **2020**, *186*, 107918. https://doi.org/10.1016/j.compscitech.2019.107918.

(38) Hertrampf; Olivares. Iron Amino Acid Chelates. *Int. J. Vitam. Nutr. Res.* **2004**, *74* (6), 435–443. https://doi.org/10.1024/0300-9831.74.6.435.

(39) Stadtman, E. R. OXIDATION OF FREE AMINO ACIDS AND AMINO ACID RESIDUES IN PROTEINS BY RADIOLYSIS AND BY METAL-CATALYZED REACTIONS. *Annu. Rev. Biochem.* **1993**, *62* (1), 797–821. https://doi.org/10.1146/annurev.bi.62.070193.004053.

(40) Mizuguchi, H.; Atsumi, H.; Hashimoto, K.; Shimada, Y.; Kudo, Y.; Endo, M.; Yokota, F.; Shida, J.; Yotsuyanagi, T. Highly Sensitive Colour Change System within Slight Differences in Metal Ion Concentrations Based on Homo–Binuclear Complex Formation Equilibrium for Visual Threshold Detection of Trace Metal Ions. *Anal. Chim. Acta* **2004**, *527* (2), 131–138. https://doi.org/10.1016/j.aca.2004.09.080.

(41) Eteshola, E. O. U.; Haupt, D. A.; Koos, S. I.; Siemer, L. A.; Morris, D. L. The Role of Metal Ion Binding in the Antioxidant Mechanisms of Reduced and Oxidized Glutathione in Metal-Mediated Oxidative DNA Damage. *Metallomics* **2020**, *12* (1), 79–91. https://doi.org/10.1039/c9mt00231f.

(42) Rabaeh, K. A.; Eyadeh, M. M.; Hailat, T. F.; Madas, B. G.; Aldweri, F. M.; Almomani, A. M.;

Awad, S. I. Improvement on the Performance of Chemically Cross-Linked Fricke Methylthymol-Blue Radiochromic Gel Dosimeter by Addition of Dimethyl Sulfoxide. *Radiat. Meas.* **2021**, *141*, 106540. https://doi.org/10.1016/j.radmeas.2021.106540.

(43) Jin, C.; Chen, J.; Yang, L.; Luo, W.; Wu, G.; Zha, Y. Effect of DMSO on the Sensitivity and Diffusion of FPGX Gel Dosimeter. *Radiat. Phys. Chem.* **2012**, *81* (7), 879–883. https://doi.org/10.1016/j.radphyschem.2012.03.002.